Proceedings of the 21st ICSMGE, Vienna, Austria, 14 – 19 June 2026. Pistrol, Adam & Schweiger (eds.)
Published by: ÖGG, Austrian Society for Geomechanics, Salzburg, Austria, ISBN 978-3-9503898-4-5
https://doi.org/10.53243/ICSMGE2026-1143

Modelling coupled seepage-erosion-deformation process using the material point method and an advanced constitutive model

Danial Haider, Zhou Chao
Department of Civil and Environmental Engineering, The Hong Kong Polytechnic University, Hong Kong,
c.zhou@polyu.edu.hk

ABSTRACT: Underground water pipeline systems are susceptible to damage from excessive fluid pressure, soil settlement, and pipeline material deterioration. The resulting damage in the form of pipeline leakage may lead to soil erosion and cause sinkholes and other geohazards, posing significant economic and infrastructural threats to society. Accurately simulating the coupled seepage-erosion-deformation processes is challenging because existing constitutive models generally do not account for stress- and porosity-dependent particle loss or fines-dependent soil behaviour, and conventional numerical techniques struggle to simulate large deformations effectively. This paper reports a two-phase (solid and liquid) multi-species two-point Material Point Method (MPM) formulation, encapsulating an advanced constitutive model within the bounding surface plasticity framework. The erosion of solid particles is modelled through phase transformation between fluidised (fines in liquid phase) and solid particles, incorporating state dependency of particle loss under complex hydraulic conditions. The proposed formulation also provides insights into spatial and temporal variations of fine particles, which are fundamental for better predictions of the mechanical behaviour of soil. In addition, the stress-strain behaviour under cyclic hydraulic and mechanical loading conditions is analysed using three coupled bounding surfaces in p'-q-i space, along with a fines-dependent critical state line in the compression plane. The new constitutive model, along with MPM's inherent capability to model large deformations, enables the proposed method to successfully simulate the coupled seepage-erosion-deformation process, such as the leakage-induced sinkhole.

KEYWORDS: Bounding surface plasticity, internal erosion, suffusion, erosion law.

1 INTRODUCTION

Underground water and sewage pipelines are vulnerable to severe damage from excess fluid pressure, soil settlement, and pipeline material deterioration (Monzer et al. 2023). As a result, water may infiltrate from the surrounding soil into the pipe, or exfiltrate from the pipe into the surrounding soil, potentially resulting in catastrophic geohazards such as sinkholes (Shiau et al. 2022). Water exfiltration exerts a drag force on the soil particles, causing movement of fine particles away from the pipe periphery or fluidisation of surrounding soil, depending on fluid pressure exerted through cracks (Chao et al. 2025; Guo et al. 2023). The resulting erosion can significantly change the mechanical properties of the soil and may lead to ground collapse. The focus of this study is on gap-graded soils due to their high susceptibility to erosion.

Several numerical methods have been developed to study seepage-induced internal erosion. Vardoulakis et al. (1996) proposed a three-phase approach (i.e., solid, fluidised solid, and fluid particles) using the finite difference method (FDM) to study sand production. Zhang et al. (2019) later applied this approach using the Finite Element Method (FEM) to investigate erosion caused by water infiltration in slope stability problems. While the proposed formulations can describe the variation of the concentration ratio of fluidised particles, they cannot easily model large deformation due to the mesh distortion. Ma et al. (2022) proposed a comprehensive five-phase approach to study seepage-induced internal erosion and the resulting deformation behaviour in the framework of smoothed particle hydrodynamics (SPH). The mechanical consequences of erosion were only considered through the linear variation of peak friction angle with the fine content. The imposition of boundary conditions in SPH is a daunting task. To address this problem while avoiding mesh tangling side by side, Lei et al. (2020) employed the generalised interpolation material point method (GIMP) using a three-phase multi-species framework to investigate the coupled seepage-erosion deformation process. The mechanical behaviour of soil was modelled through the Mohr-Coulomb model without considering the effect of fine content on the soil properties for simplicity, even though experimental studies have shown a decreased dilative tendency and a rise in the critical state line with increased internal erosion (Chen et al. 2016). In summary, while previous studies provide a conceptual framework for modelling seepage-induced internal erosion, it is necessary to improve the relevant constitutive models and numerical techniques to better capture this complex process.

In this study, a two-phase, two-point and multi-species MPM formulation has been developed, which considers the erosion of fine particles and its influence on the mechanical behaviour of soil. For the numerical framework, the MPM has been chosen because it combines the advantages of both point-based and mesh-based methods, and the presence of a background grid facilitates the imposition of boundary conditions. First, the MPM framework is presented, followed by the erosion law and the bounding surface plasticity model. Finally, the MPM formulation is applied to a 0.5 m soil column subjected to hydraulic loading to investigate the spatial-temporal evolution of erodible fines and liquidised fines, as well as its mechanical consequences.

2 MPM-BASED NUMERICAL MODEL

2.1 *MPM framework*

In this study, saturated soil is conceptualised as a two-phase, multi-species porous medium, as illustrated in Figure 1. The solid phase is assumed to consist of two species: coarse particles and erodible fines. The liquid phase comprises water and liquidised fines. The continuum body is divided into 'N' sub-domains, each represented by two sets of material points corresponding to the solid and liquid phases, respectively. These material points carry all relevant information for their respective phases and species, such as mass, momentum, stress, loading history, erodible fine content, and liquidised fines. The terms porosity (n), fine content (F_c), and concentration ratio (c^e) are used to describe the volume fractions of the two phases and their respective species. The volume fractions for the solid phase, liquid phase, erodible fines, and liquidised fines are $1-n$, n, $(1-n)F_c$, and nc^e, respectively. Phase transitions between the solid and liquid phases are considered to model the erosion and deposition of fines, based on hydraulic loading and

soil state, as governed by the erosion law discussed in a later section. Fines that enter the liquid phase are assumed to move with the water, sharing the same velocity. In cases of high-pressure water flow, fluidisation becomes the dominant phenomenon. The soil is considered fluidised when the mean effective stress reaches zero (the soil loses its shear strength) and porosity reaches the maximum threshold value. In developing these equations, the liquid particles are assumed to be weakly compressible.

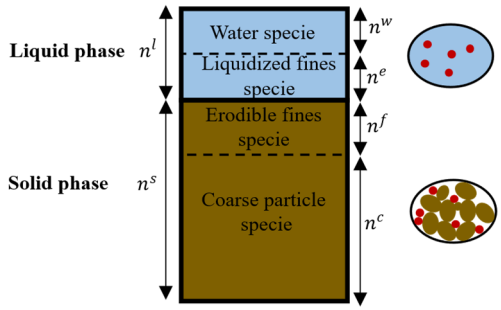

Figure 1. Phase diagram of two-phase and multi-species porous medium.

2.2 *Governing equations*

2.2.1 *Conservation of momentum equations*

This study employs the momentum balance equations for both the liquid phase and the mixture to determine the accelerations of the liquid and solid phases. The momentum balance equation for the liquid phase can be written as follows:

$$n^l\rho^l\dot{\boldsymbol{v}}^l = -n^l\nabla p^l - \boldsymbol{F}_d^l + n^l\rho^l\boldsymbol{g} \tag{1}$$

where ρ^l represents the liquid phase density, $\dot{\boldsymbol{v}}^l$ represent the liquid phase acceleration, ∇p^l corresponds to the spatial gradient of pore water pressure, and $\boldsymbol{g}$ represents the body force. The term $\boldsymbol{F}_d^l$ represents the drag force imposed by solid-liquid phase interaction and is given by Lei et al. (2020) as follows:

$$\boldsymbol{F}_{\boldsymbol{d}}^{\boldsymbol{l}} = \frac{(n^l)^2\rho^l g}{k^l}(\boldsymbol{v}^l - \boldsymbol{v}^s) \tag{2}$$

where k^l represents the permeability of the soil, $\boldsymbol{v}^l$ represents the liquid phase velocity, and $\boldsymbol{v}^s$ represents the solid phase velocity. Under high-pressure exfiltration from the pipe, the linear relationship between the drag force and relative velocity needs modification to account for turbulent flow. The drag force term becomes zero when only liquid material points are present in the domain (i.e., in the case of free water).

To determine the acceleration of the solid phase, the momentum balance equation for the solid-fluid mixture is utilised, given by:

$$(1-n)\rho^s\dot{\boldsymbol{v}}^s + nS^l\rho^l\dot{\boldsymbol{v}}^l = \mathrm{div}(\boldsymbol{\sigma}^{\mathrm{T}}) + (1-n)\rho^s\boldsymbol{g} + nS^l\rho^l\boldsymbol{g} \tag{3}$$

where ρ^s represents the solid phase density, $\dot{\boldsymbol{v}}^s$ represents the acceleration of the solid phase, and $\boldsymbol{\sigma}$ represents the Cauchy stress tensor. Balance of angular momentum results in $\boldsymbol{\sigma} = \boldsymbol{\sigma}^{\mathrm{T}}$.

2.2.2 *Conservation of mass balance*

The mass balance equation for the solid phase, incorporating the solid–liquid phase mass transition, can be written as:

$$\frac{\mathrm{d}^s}{\mathrm{d}t}[(1-n)\rho^s V] = \frac{(1-n)\rho^s V}{1-F_c}\frac{\mathrm{d}^s}{\mathrm{d}t}[F_c] \tag{4}$$

Compared to existing equations, the expression on the right side of the above equation considers the mass loss due to the phase transition of fines under hydraulic loading. Similarly, mass balance equations for the water and liquidised fine species are given by the following equations:

$$\frac{\mathrm{d}^l}{\mathrm{d}t}[m^w] = \frac{\mathrm{d}^l}{\mathrm{d}t}[(1-c^e)nS^l\rho^w V] = 0 \tag{5}$$

$$\frac{\mathrm{d}^l}{\mathrm{d}t}[c^e nS^l\rho^e V] = -\frac{(1-n)\rho^s V}{1-F_c}\frac{\mathrm{d}^s}{\mathrm{d}t}[F_c] - \nabla(1-n)F_c\rho^s V\cdot(v^l - v^s) \tag{6}$$

Furthermore, spatial discretisation of the momentum balance equations for the liquid phase and solid-fluid mixture, the mass balance of liquidised fines, and the erosion law was performed by first deriving the weak form of each equation. Standard MPM basis functions were then used to interpolate the field variables and test functions. For time discretisation, an explicit time integration scheme was adopted.

3 EROSION LAW

Existing models relating particle removal to the hydraulic gradient or water velocity rarely account for the state-dependent nature of particle detachment.(Cividini and Gioda 2004; Zhang et al. 2019). In this study, a new formulation is employed, which explicitly incorporates the effects of mean stress level and void ratio on the fine removal process. For coarse-grained soils—where the coarser particles govern mechanical behaviour—the erosion rate is defined relative to the coarse fraction as follows:

$$\frac{dCF}{dt} = \mu\, i_m(CF_u - CF) \tag{7}$$

$$CF_u = \begin{cases} CF_0 & 0 \le i_m \le i_{\mathrm{cr}} \\ CF_0 + \alpha[\log(i_m - i_{cr} + 1)]^\beta & i_m > i_{\mathrm{cr}} \end{cases} \tag{8}$$

where CF_u represents the ultimate coarse fraction attainable at a hydraulic gradient i_m, μ governs the time evolution of change in the coarse fraction to achieve CF_u, CF_0 corresponds to the initial coarse fraction of the soil before erosion, i_{cr} represent the threshold hydraulic gradient, and α and β are material parameters. The state-dependent nature of the erosion process is incorporated by accounting for the linear variation of the critical hydraulic gradient and the erosion sensitivity parameter α with the void ratio and mean stress level, respectively.

4 CONSTITUTIVE MODEL

In this study, a novel bounding surface plasticity framework is employed to model the mechanical consequences of internal erosion and post-erosion behaviour. The removal of fines alters the soil gradation, resulting in a shift of the critical state line (CSL) that governs the soil's compression behaviour. This effect is captured through a coarse-fraction-dependent CSL. Furthermore, erosion of fines induces soil deformation under constant stress conditions, which is modelled via three interrelated bounding surfaces in the p'-q-i space. The model uses five variables to define the state of the soil: mean effective stress, deviatoric stress, specific volume, coarse fraction, and hydraulic gradient. In addition, the effect of the current state with reference to the critical state on peak shear strength and dilatancy behaviour of the soil is incorporated through formulations proposed by Dafalias and Manzari (2004). Additional model details are provided in subsequent sections.

4.1 *Critical state and normal compression line*

Various experimental studies have shown that the critical state line (CSL) shifts upward in the v -$ln\ p'$ plane with increasing coarse fraction, while its effect on the critical state stress ratio in the p'-q plane remains minimal (Mehdizadeh et al. 2021). To model this coarse-fraction-dependent CSL in v -$ln\ p'$, the following relationships are employed:

$$v_{cs} = \Gamma_{CF} - \omega \ln\left(\frac{p'}{p_{ref}}\right) \tag{9}$$

$$\Gamma_{CF} = \Gamma_{100} - \zeta(1 - CF) \tag{10}$$

where the parameter ζ governs the linear variation of the CSL intercept with the percentage of coarse fraction, Γ_{100} corresponds to the CSL intercept of soil with a 100% coarse fraction and M is the stress ratio at the critical state. For simplicity, a similar relationship has been considered to model the effect of coarse fraction on the normal compression line.

4.2 *Bounding surfaces*

Three bounding surfaces are introduced to model: (1) the removal of fines and consequent increase in coarse fraction, (2) erosion-induced deformation, and (3) post-erosion behaviour of soil, while accounting for erosion history effects. The first bounding surface, governing the erosion process itself, is defined as follows:

$$F_i = i - \max\{i_{cr},\ i_m\} \tag{11}$$

where i denotes the current hydraulic gradient, i_m represents the maximum hydraulic gradient, soil has experienced in the past, and i_{cr} is the critical hydraulic gradient for erosion initiation. When $i < i_{cr}$, coarse fraction remains constant. Otherwise, the evolution of the coarse fraction is governed by both the current hydraulic gradient and erosion history (captured through the parameter i_m).

The second bounding surface, describing the compression mechanism, is defined as:

$$F_c = p' - p'_{0(CF)} \tag{12}$$

where p' is the current mean effective stress and $p'_{0(CF)}$ denotes the preconsolidation stress computed from the coarse fraction-dependent NCL. Experimental evidence indicates that the reduction in specific volume during erosion exceeds the vertical translation of the NCL in the v-$ln\ p'$, thereby reducing the preconsolidation stress (Chang, 2012; Muir Wood et al. 2010). This triggers a transition from an over-consolidated to a lightly over-consolidated state, inducing soil skeleton deformation as it cannot sustain the current stress state without additional volumetric strains.

The third bounding surface, governing the shearing mechanism, is defined as follows:

$$F_s = q - M_m p' \tag{13}$$

where M_m denotes the apparent maximum stress ratio and serves as a hardening parameter that controls the evolution of the bounding surface. This hardening parameter evolves with both volumetric strains caused by shearing and changes in coarse fraction, enabling the model to capture erosion-induced deformation under constant stress conditions. Its variation with changes in coarse fraction is given by:

$$\frac{\partial M_m}{\partial CF} = -(a_0 + b_0\eta)e^{c_0 p'} \tag{14}$$

Details of the flow rule and mapping rule employed in this study can be found in (Zhou et al. 2015).

4.3 *Model validation*

Model performance was evaluated by comparing the computed results with experimental data from triaxial tests on gap-graded soil (mixture of CDG and Leighton Buzzard sand) subjected to internal erosion, as reported by Chang (2012). Figure 2 shows the change in coarse fraction with hydraulic gradient for soils under different mean effective stress levels. The model is able to capture the evolution of the coarse fraction. Figure 3 and Figure 4 present the post-erosion mechanical behaviour of the soil subjected to erosion in Figure 2. When the post-erosion drained triaxial test results were compared with benchmark test data, the model successfully captured the transition from strain softening to strain hardening, as well as the change in volumetric response from dilative to contractive. The small variation in the predicted volumetric response is attributed to uncertainties in determining the CSL parameters.

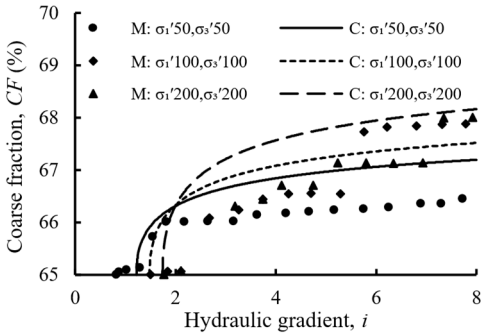

Figure 2. Coarse fraction evolution in triaxial specimens subjected to various mean stress levels.

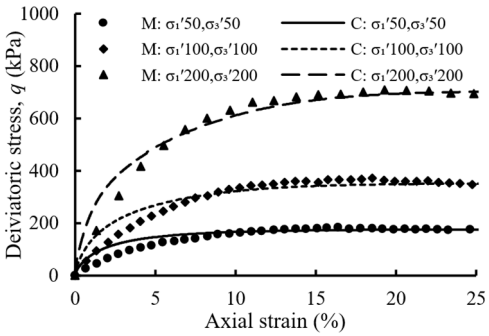

Figure 3. Stress–strain response of soil after erosion under different stress states.

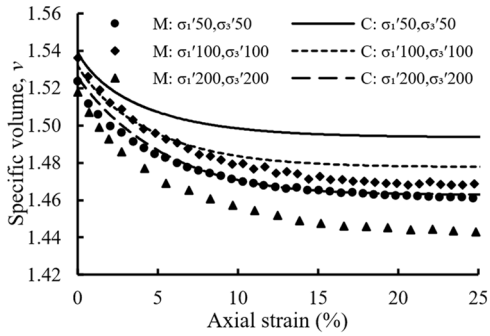

Figure 4. Volumetric response of eroded soil during drained triaxial shear testing.

5 SIMULATION OF 1-D COLUMN TEST

To evaluate the capability of the proposed method in simulating the coupled seepage-erosion-deformation process, a 0.5 m soil column was subjected to pressure-controlled water inflow using in-house code. The soil column was discretised into cells

measuring 0.02 m × 0.02 m, with each cell containing four material points (MPs) for both the liquid and solid phases. The initial stress state of the soil was established by allowing the system to reach equilibrium under gravity. The model parameters were calibrated using test results from triaxial specimens subjected to internal erosion, as reported by Chang (2012). At time $t = 0$, a prescribed pressure of 7500 Pa was applied at the bottom of the soil column to achieve a hydraulic gradient of 0.5 at steady state. Figure 5 shows the spatial-temporal evolution of fine content and the concentration ratio of liquidised fines. It can be observed that the change in fine content is greater at the bottom of the soil column compared to the top. This is because, when the prescribed pressure is applied at the bottom, the hydraulic gradient initially exceeds 0.5, leading to greater particle loss in that region. After continuous water flow from the bottom to the top of the soil column, a stage is reached where there are no liquidised fines remaining in the soil column, thanks to the capability of the two-phase, two-point MPM framework. Figure 6 shows the distribution of porosity and effective plastic strain along the soil column. In the case where erosion was not considered, porosity increased slightly from 0.33 to 0.335 due to a decrease in mean effective stress. However, when erosion was considered, porosity increased significantly by 2.5%. These results truly reflect the behaviour of soil undergoing erosion.

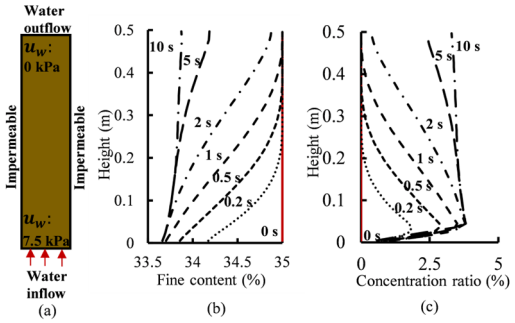

Figure 5. (a) 1-D column test setup and spatial-temporal evolution of (b) fine content and (c) concentration ratio along the soil column.

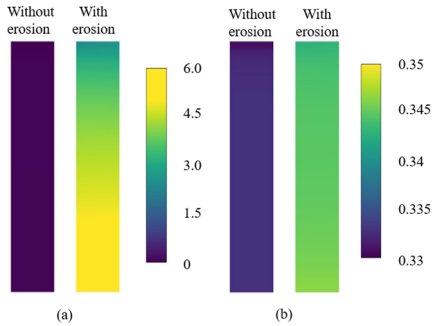

Figure 6. Comparison of (a) plastic strain (%) and (b) porosity variation during water infiltration with and without erosion of fines.

6 SUMMARY AND CONCLUSION

In this study, two-phase, two-point and multi-species MPM formulations have been presented to model the coupled seepage-erosion-deformation process. Under low-pressure leakage from the pipeline, this framework considers the phase transition of fine particles from the solid to the liquid phase. A novel state-dependent erosion law enables the formulation to govern phase transitions and monitor the spatial-temporal evolution of fines and liquidised fines. Monitoring the fine content provides information related to the coarse fraction, which governs the mechanical behaviour of the soil. The application of a new bounding surface model within the MPM framework enables the simulation of erosion-induced deformation and the resulting changes in porosity. This framework can also capture soil fluidisation under high-pressure exfiltration by setting a threshold porosity and considering the deviatoric part of the water phase stress tensor, thereby treating the solid-fluid mixture as a viscous fluid. In conclusion, the incorporation of a two-phase, two-point formulation, while considering the phase transition of fines by an erosion law, and a novel constitutive model, provides a comprehensive framework for studying sinkhole formation due to pipeline leakage in detail.

7 ACKNOWLEDGEMENTS

The authors would like to thank the Research Grants Council (RGC) of the HKSAR for providing financial support through grants N_PolyU526/23 and 15205721.

8 REFERENCES

Chang, D. 2012. *Internal erosion and overtopping erosion of earth dams and landslide dams*. The Hong Kong University of Science and Technology.

Chao, H., Tan, Y., and Su, Z.K. 2025. Ground failure and soil erosion caused by bursting of buried water pipeline: experimental and numerical investigations. *Engineering failure analysis* 167**,** 108965.

Chen, C., Zhang, L. M., and Chang, D. S. 2016. Stress-Strain Behavior of Granular Soils Subjected to Internal Erosion. *Journal of geotechnical and geoenvironmental engineering* 142 (12).

Cividini, A., and Gioda, G. 2004. Finite-Element Approach to the Erosion and Transport of Fine Particles in Granular Soils. *International journal of geomechanics* 4 (3)**,** 191-198.

Dafalias, Y. F., and Manzari, M. T. 2004. Simple Plasticity Sand Model Accounting for Fabric Change Effects. *Journal of engineering mechanics* 130 (6)**,** 622-634.

Guo, S., Jiang, Y., Tang, Y., Cheng, H., Luo, X., Lv, Y., and Li, M. 2023. Experimental study on the soil erosion through a defective pipe under the cyclic infiltration-exfiltration flow. *Transportation Geotechnics* 42**,** 101085.

Lei, X., He, S., Chen, X., Wong, H., Wu, L., and Liu, E. 2020. A generalised interpolation material point method for modelling coupled seepage-erosion-deformation process within unsaturated soils. *Advances in water resources* 141**,** 103578.

Ma, G., Bui, H. H., Lian, Y., Tran, K. M., and Nguyen, G. D. 2022. A five-phase approach, SPH framework and applications for predictions of seepage-induced internal erosion and failure in unsaturated/saturated porous media. *Computer methods in applied mechanics and engineering* 401**,** 115614.

Mehdizadeh, A., Disfani, M. M., and Shire, T. 2021. Post-erosion mechanical response of internally unstable soil of varying size and flow regime. *Canadian geotechnical journal* 58 (4)**,** 531-539.

Monzer, A., Faramarzi, A., Yerro, A., and Chapman, D. 2023. MPM Investigation of the Fluidization Initiation and Postfluidization Mechanism around a Pressurized Leaking Pipe. *Journal of geotechnical and geoenvironmental engineering* 149 (11).

Muir Wood, D., Maeda, K., and Nukudani, E. 2010. Modelling mechanical consequences of erosion. *Géotechnique* 60 (6)**,** 447-457.

Shiau, J., Mahalingasivam, K., Chudal, B., and Keawsawasvong, S. 2022. Pipeline Burst–Related Soil Stability in Collapse Condition. *Journal of pipeline systems* 13 (3).

Vardoulakis, I., Stavropoulou, M., and Papanastasiou, P. 1996. Hydro-mechanical aspects of the sand production problem. *Transport in porous media* 22 (2)**,** 225-244.

Zhang, L., Wu, F., Zhang, H., Zhang, L., and Zhang, J. 2019. Influences of internal erosion on infiltration and slope stability. *Bulletin of engineering geology and the environment* 78 (3)**,** 1815-1827.

Zhou, C., Ng, C. W. W., and Chen, R. 2015. A bounding surface plasticity model for unsaturated soil at small strains. *International Journal for Numerical and Analytical Methods in Geomechanics* 39 (11)**,** 1141-1164.